NMR Structure of Human Apolipoprotein C-II in the Presence of Sodium Dodecyl Sulfate†

Christopher A. MacRaild, Danny M. Hatters, Geoffrey J. Howlett, and Paul R. Gooley*

Russell Grimwade School of Biochemistry and Molecular Biology, University of Melbourne, Gate 12, Royal Parade, Parkville, Victoria 3052, Australia

Received December 13, 2000; Revised Manuscript Received February 27, 2001

ABSTRACT: The structure and protein−detergent interactions of apolipoprotein C-II (apoC-II) in the presence of SDS micelles have been investigated using circular dichroism and heteronuclear NMR techniques applied to ^{15}N-labeled protein. Micellar SDS, a commonly used mimetic of the lipoprotein surface, inhibits the aggregation of apoC-II and induces a stable structure containing approximately 60% α-helix as determined by circular dichroism. NMR reveals the first 12 residues of apoC-II to be structurally heterogeneous and largely disordered, with the rest of the protein forming a predominantly helical structure. Three regions of helical conformation, residues 16−36, 50−56, and 63−77, are well-defined by NMR-derived constraints, with the intervening regions showing more loosely defined helical conformation. The structure of apoC-II is compared to that determined for other apolipoproteins in a similar environment. Our results shed light on the lipid interactions of apoC-II and its mechanism of lipoprotein lipase activation.

Apolipoprotein C-II (apoC-II)[1] is a 79 residue exchangeable apolipoprotein that plays an essential role in plasma lipid transport and metabolism. ApoC-II is a protein cofactor for lipoprotein lipase (LpL), an enzyme that hydrolyzes triacylglycerol during the metabolic remodeling of chylomicrons and very low-density lipoproteins (*1*, *2*). As with the other exchangeable apolipoproteins, apoC-II binds reversibly to the polar lipid surface of plasma lipoprotein particles in vivo and associates with a range of natural and synthetic lipid surfaces in vitro with a concomitant change in secondary structure (*3*). Analysis of this conformational change and amino acid sequence analysis of apoC-II and other exchangeable apolipoproteins have led to the generally accepted hypothesis that exchangeable apolipoproteins associate with lipid surfaces by means of amphipathic helical regions believed to be present in all members of the family (*4*). The results of a number of studies have localized the lipid binding activity of apoC-II to a region in the N-terminal half of the protein with a strongly amphipathic nature and possibly to a second smaller region at the C-terminus (*5*−*7*).

Activation of LpL is believed to involve the capacity of apoC-II to bind LpL as a binary protein−protein complex and stabilize a ternary complex with the lipoprotein substrate by means of the apoC-II lipid binding regions (*8*). It has also been suggested that apoC-II binding might induce a change in LpL conformation which exposes the active site to substrate in a manner analogous to the interaction of pancreatic lipase with its protein cofactor, colipase (*9*). However, in the absence of detailed structural information on apoC-II and its interactions with lipid and LpL, the details of this model remain controversial.

ApoC-II in lipid-free solution has long been known to self-associate, and recently this association was shown to result in the formation of amyloid-like fibrils (*10*). The presence of phospholipid surfaces or sodium dodecyl sulfate (SDS) micelles inhibits amyloid formation. It has been suggested that in the absence of lipid apoC-II adopts a less-ordered structure that is prone to conformational changes leading to amyloid formation, whereas the presence of lipid stabilizes α-helical conformations and protects against the formation of amyloid-like β-sheet structures (*10*). A number of other apolipoproteins have been shown to form amyloid fibrils in vivo (*11*−*13*), and amyloid has been identified in atherosclerotic plaques (*14*, *15*). Structural detail of apoC-II in its lipid-bound form may provide valuable insight into the process of amyloid fibril formation by apoC-II and apolipoproteins in general and might suggest mechanisms to prevent its occurrence in vivo.

Previous structural studies of apoC-II have focused on C-terminal fragments in the helix inducing solvent 1,1,1,3,3,3-hexafluoro-2-propanol (HFP) (*16*, *17*), or bound to SDS micelles (*18*). SDS micelles are commonly used mimics of membrane and lipoprotein environments for NMR studies of lipid-associating proteins (*19*). Both of these studies suggest the presence of a well-defined helix across residues 67−74 that is C-terminally capped with a turn-like structure comprising residues 76−79. N-terminal to this helix lies an unstructured region followed by a second, poorly defined helix spanning residues 50−58.

† This work was funded by the National Health and Medical Research Council and the Australian Research Council. C.A.M. is the recipient of an Australian Postgraduate Award. D.M.H. is the recipient of a Melbourne Research Scholarship.

* Correspondence should be addressed to this author. Phone: +61 3 8344 5935; Fax: +61 3 9347 7730; Email: prg@unimelb.edu.au.

[1] Abbreviations: apoC-II, apolipoprotein C-II; LpL, lipoprotein lipase; SDS, sodium dodecyl sulfate; HFP, 1,1,1,3,3,3-hexafluoro-2-propanol; NMR, nuclear magnetic resonance; CD, circular dichroism; HSQC, heteronuclear single-quantum coherence; HMQC, heteronuclear multiple-quantum coherence; NOESY, nuclear Overhauser effect spectroscopy; TOCSY, total correlation spectroscopy; NOE, nuclear Overhauser effect.

10.1021/bi002821m CCC: $20.00
Published on Web 04/10/2001

We have prepared uniformly ^{15}N-enriched recombinant human apoC-II, allowing NMR spectral assignment and structural determination of residues 13−79 of the intact protein. This study provides the first high-resolution structural information available for intact human apoC-II. It indicates an extensive region of α-helix in the N-terminal half of the protein that shares a number of structural features with the lipid binding regions of other apolipoproteins. It also presents a more detailed structure for the C-terminal region, affording new insights on the mechanism of LpL activation.

MATERIALS AND METHODS

Expression and Purification of ApoC-II. ApoC-II was bacterially expressed (*20*) and purified as previously described (*10*). For ^{15}N enrichment of apoC-II, BL21(DE3) competent cells transformed with the pET-11a/apoC-II construct were grown overnight in 100 mL of modified M9 media, containing 100 μg/mL ampicillin with $^{15}NH_4Cl$ as the only nitrogen source. This culture was used to inoculate 1 L of modified M9 media (*21*) containing 1 g of $^{15}NH_4Cl$ and 100 μg/mL ampicillin in a Braun BIOSTAT B1 fermentor at 37 °C. The culture was maintained at pH 6.8 by addition of 2 M NaOH. Air was pumped into the culture at 8 L/min, and the level of dissolved O_2 was maintained at 12.5% saturation by regulation of the stirring rate. Expression of apoC-II was induced by the addition of 1 mM IPTG when the A_{600} values for the cell culture reached 2.5−3.0, at which point a further 1.5 g of $^{15}NH_4Cl$ was added. Cells were harvested after approximately 2 h of expression, and apoC-II was purified as for unlabeled material.

Circular Dichroism. Circular dichroism (CD) spectra of apoC-II in SDS were acquired using a Jasco J-720 spectropolarimeter and 0.1 mm path length quartz cuvettes. Stocks of apoC-II at 18.4 mg/mL in 5 M urea were diluted into 20 mM sodium acetate, pH 5.0, with 30.3 mM SDS to a final protein concentration of 1.5 mg/mL. Data points were collected at 0.5 nm intervals with 0.5 s integration times and a 1 nm spectral bandwidth. Four spectra were collected for each sample and averaged before correction against buffer containing the appropriate concentration of SDS. The percentage of α-helix present for each sample was estimated using the relation: % helix = $(3000 - [\theta]_{222\ nm})/39000$, where $[\theta]_{222\ nm}$ is the mean residue ellipticity at 222 nm (*22*).

NMR Spectroscopy. Samples for NMR spectroscopy were prepared by dissolving lyophilized apoC-II in 550 μL of 220 mM SDS, 20 mM sodium acetate, pH 5, 10% D_2O/90% H_2O to a final protein concentration of 1.8 mM. Samples also contained 0.1% sodium azide. Chemical shifts were referenced against 2,2-dimethyl-2-silapentane-5-sulfonic acid. The stability of these samples was monitored by ^{1}H,^{15}N-HSQC experiments, and no changes were observed over a period of several months storage at room temperature. NMR spectroscopy was performed on a Varian Inova 500 MHz NMR spectrometer equipped with a pulsed field gradient triple resonance probe and z gradient. Two-dimensional ^{1}H,^{15}N-HSQC spectra (*23*) were obtained at 25 and 40 °C using a spectral width of 6255.4 Hz and 1024 complex points in the ^{1}H dimension and a spectral width of 1200 Hz in the ^{15}N dimension with 128 t_1 increments. ^{1}H,^{15}N-NOESY−HSQC and TOCSY−HSQC spectra (*24*−*26*) were acquired from the same sample at 40 °C. The spectral widths were 5599.9, 5000.0, and 1350.0 Hz in F1 (^{1}HN), F2 (^{1}H), and F3 (^{15}N), respectively, with 512, 128, and 32 complex points. Carrier frequencies were 4.58 ppm for proton and 118 ppm for ^{15}N. Mixing times were between 75 and 150 ms for the NOESY experiments, and 65 ms for the TOCSY experiment. Three-dimensional sensitivity-enhanced HNHA and HNHB experiments (*27*, *28*) were performed under identical conditions with carrier frequencies of 4.58 ppm in the proton dimension and 114 ppm in the ^{15}N dimension. Spectral widths of 5602.2, 2500.0, and 800.0 Hz were used in F1 (^{1}HN), F2 (^{1}H), and F3 (^{15}N), respectively, with 512, 72, and 28 complex points. To resolve NOEs between backbone amides of degenerate ^{1}HN chemical shift, a 3D HMQC−NOESY−HSQC experiment (*29*) was recorded at 40 °C using spectral widths of 5599.9, 1350.0, and 1350.0 Hz, and 512, 32, and 32 complex points in F1 (^{1}HN), F2 (^{15}N), and F3 (^{15}N). For HMQC−NOESY−HSQC, water suppression was achieved by the WATERGATE technique (*30*), and gradient selection was used for all other experiments. Data were processed using NMRPipe (*31*) on LINUX workstations running REDHAT 6.0. A solvent filter was applied followed by processing using a 70° shifted sine-bell squared window function. FIDs were zero-filled prior to Fourier transformation and baseline correction. Linear prediction was applied in ^{15}N as appropriate. The software packages XEASY (*32*) and NMRDRAW (*31*) were used for all spectral analysis.

Spectral Assignment. Backbone assignment of apoC-II was achieved using the ^{1}H,^{15}N-NOESY−HSQC, ^{1}H,^{15}N-HMQC−NOESY−HSQC, and ^{1}H,^{15}N-TOCSY−HSQC spectra. Due to the α-helical nature of the protein, strong sequential NH−NH connectivities were observed in the ^{1}H,^{15}N-NOESY−HSQC spectra, facilitating assignment by extended amide−amide walks. Discontinuities in amide−amide walks due to HN chemical shift degeneracy were resolved by means of ^{1}H,^{15}N-HMQC−NOESY−HSQC cross-peaks. Assignment of aliphatic side-chain protons was achieved using the ^{1}H,^{15}N-TOCSY−HSQC, HNHA and HNHB spectra, and sequential NOEs in the ^{1}H,^{15}N-NOESY−HSQC spectra involving side-chain atoms were used to confirm the backbone assignments made on the basis of amide−amide connectivities. No attempt was made to assign the four prolines of apoC-II, side-chain NH_2 groups, or aromatic protons. $^3J_{\alpha H-NH}$ coupling constants, and hence ϕ torsion angles, were determined from the HNHA spectrum (*27*). Secondary chemical shifts for αH and NH protons were calculated using the random coil chemical shift values of Wüthrich (*33*).

Structure Calculations. The software package DYANA (*34*) was used for the collation of structural constraints. NOE cross-peak intensities from the ^{1}H,^{15}N-NOESY−HSQC and HMQC−NOESY−HSQC spectra were converted to upper limit distance constraints calibrated such that the average sequential amide−amide distance constraint over the region of residues 26−35 was 2.8 Å. Only NOEs from 75 ms mixing time experiments were used in the calculation of distance constraints. Constraints about the ϕ torsion angle were derived from $^3J_{\alpha H-NH}$ coupling constants in the following manner: for residues with $^3J_{\alpha H-NH}$ less than 4 Hz, ϕ was constrained to lie between −30° and −75°; for coupling constants between 4 and 6 Hz, the bounds on ϕ were −40° and −90°. No constraint was included for residues with $^3J_{\alpha H-NH}$ greater than 6 Hz or for which resonance overlap precluded the determination of the coupling constant. The

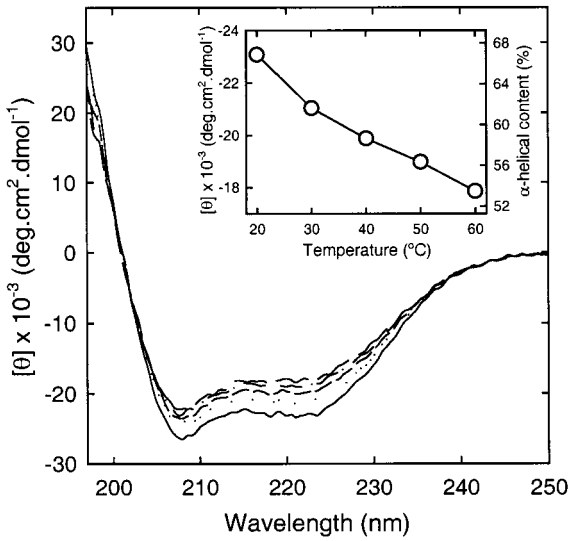

FIGURE 1: Circular dichroism spectra of 1.5 mg/mL apoC-II in 20 mM sodium acetate, pH 5.0, 30.3 mM SDS recorded at 20 (—), 30 (···), 40 (- - -), 50 (— ·· —), and 60 °C (— —). The temperature dependence of the CD signal at 222 nm (left axis) and the estimated helical content (right axis) are shown in the inset.

resulting constraints served as input to structure calculations using torsion angle dynamics simulated annealing in CNS 0.9 (*35*). A total of 100 trial structures were calculated from extended chain starting conformers with different randomly assigned initial velocities. In the final Cartesian dynamics, refinement step force constants of 50 kcal/mol for NOE constraints and 200 kcal mol^{-1} rad^{-2} for dihedral angle constraints were used. A final bundle of 22 structures is selected from the trial structure set by selecting those structures without NOE violations greater than 0.35 Å and with Lennard−Jones energies less than −55 kcal/mol.

RESULTS

Circular Dichroism. The far-UV circular dichroism spectra of apoC-II in the presence of a 180-fold molar excess of SDS display the characteristic features of α-helical structure, namely, minima at 208 and 222 nm and sharply increasing ellipticity at wavelengths below 205 nm (Figure 1). The magnitude of the minimum at 222 nm was indicative of a helical content of approximately 60% at 40 °C, with relatively small variation observed over the temperature range 20−60 °C. Previous studies have shown that the concentration of residual urea present in these samples (approximately 400 mM) has no significant effect on the CD spectrum of lipid-bound apoC-II (D. Hatters, unpublished results). The insolubility of apoC-II at acidic pH prevents direct comparison with apoC-II in the absence of SDS; however, freshly prepared apoC-II at neutral pH displays spectral characteristics typical of predominantly disordered structure, with a slow time-dependent increase in β content corresponding to amyloid formation (*10*). The CD spectra seen here are similar to those seen for apoC-II bound to phospholipid vesicles (data not shown).

NMR Spectral Assignment and Structural Constraints. Two- and three-dimensional NMR spectra of ^{15}N-labeled human apoC-II were acquired in the presence of SDS at 40 °C and pH 5.0. As is typical for α-helical proteins, the chemical shift dispersion of backbone amide protons of

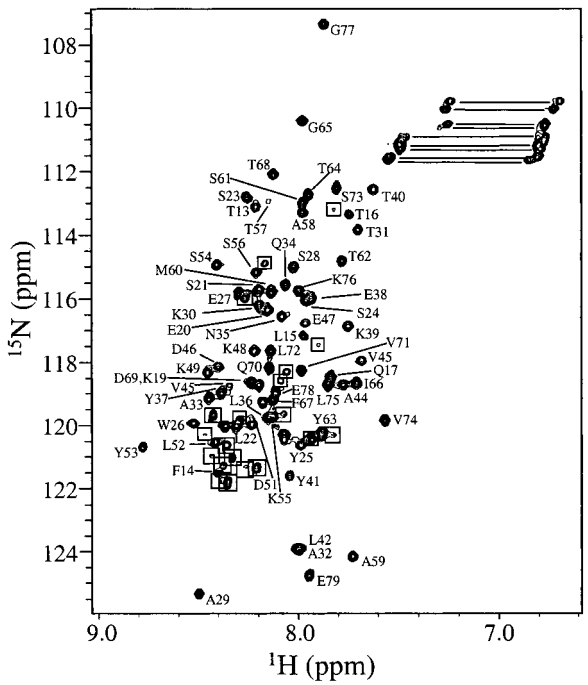

FIGURE 2: ^{1}H,^{15}N-HSQC spectrum of apoC-II in the presence of a 1:120 molar ratio of SDS in 20 mM sodium acetate, pH 5.0 at 40 °C. The peak due to the indole NH of Trp 26 which resonates at 9.96 and 126.6 ppm in ^{1}H and ^{15}N, respectively, has been excluded from the figure for clarity. Asn and Gln side-chain NH_2 groups are identified as paired high-field ^{1}H signals with identical ^{15}N chemical shifts. Backbone amide resonances are labeled with their assigned residue. Unassigned backbone amide resonances are boxed.

apoC-II is poor; however, significant dispersion in the ^{15}N dimension allows adequate resolution of almost all ^{1}H,^{15}N-HSQC cross-peaks (Figure 2). Some 89 backbone amide peaks are resolved, as compared to the 74 expected on the basis of the primary sequence of apoC-II. The additional peaks are likely due to structural heterogeneity resulting in two or more distinct conformational states for some residues of apoC-II. Despite the poor HN chemical shift dispersion and apparent structural heterogeneity, sequential assignment of backbone amides, α-protons, and most aliphatic side-chain protons for residues 13−79 was achieved. The unassigned spin systems generally exhibited very few interresidue NOE cross-peaks and weak or absent intraresidue NOEs, preventing further spectral assignment and indicating a lack of structural definition for the corresponding residues. Approximately 25 backbone amide resonances remain unassigned in the HSQC, many of which are of reduced intensity, suggesting that the corresponding residues are present in multiple conformational states. The N-terminal 12 residues of apoC-II are proline rich (the sequence of this region is TQQPQQDEMPSP), and although they may have a role in cellular processing and export (*36*), these residues fall outside of the regions of apoC-II believed to be structurally or functionally important in plasma lipid metabolism. It seems likely, therefore, that residues 1−12 are relatively unstructured and that they are the primary source of the structural heterogeneity inferred from the ^{1}H,^{15}N-HSQC spectra.

Following side-chain assignment, numerous sequential and medium-range NOEs were readily assigned. Figure 3 summarizes the short- and medium-range NOEs observed. The richness of medium-range NOEs, particularly $d_{\alpha N}(i,i+3)$ and $d_{\alpha N}(i,i+4)$, and the strong $d_{NN}(i,i+1)$ and weak $d_{\alpha N}(i,i+1)$

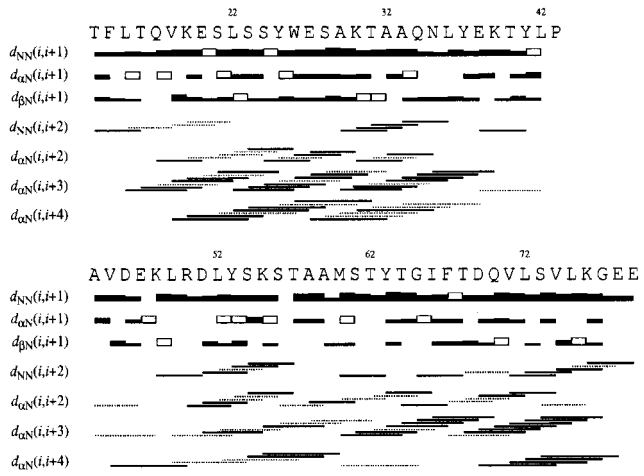

FIGURE 3: Summary of the sequential and medium-range constraints used in structural calculations. Unambiguously assigned sequential distance constraints are represented as solid bars with the height indicative of the strength of the corresponding NOE, with open bars indicating NOEs which are ambiguous due to resonance overlap and have not been included in structural calculations. Medium-range constraints are represented as solid lines, with dotted lines indicating ambiguous constraints.

NOEs over residues 16−38 and 61−76 indicate stable helical conformations for these regions.

Secondary chemical shifts for Hα and HN resonances are shown in Figure 4A. Negative Hα secondary shifts consistent with helical conformations are seen across regions 13−40 and 44−75, and the HN chemical shift shows a 3−4 residue periodic variation over residues 25−38 and 45−52, suggestive of amphipathic helices over this region.

No long-range NOEs indicative of tertiary interactions were identified, although helix−helix interactions are most likely to result in side-chain−side-chain interactions which cannot be observed by the ^{15}N-edited NOESY experiments employed here, so the possibility of tertiary interactions cannot be completely discounted.

The Fold of Human ApoC-II. CNS calculations using constraints derived from measured NOE connectivities and *J*-couplings as summarized in Figures 3 and 4B were used to derive detailed structures of apoC-II. Of 100 calculated structures, 22 were accepted for further analysis on the basis of distance constraint violations and Lennard−Jones energies. A summary of the structural statistics for this family of structures is also presented in Table 1. Analysis of the average backbone (ϕ and ψ) torsion angles for the calculated structures shows values consistent with a helical conformation across regions 15−36 and 51−76 (Figure 4C). The order parameters associated with these values reflect the variance in torsion angles across the family of structures and are presented in Figure 4D. Order parameters close to unity, indicating well-defined torsion angles, are seen over regions 17−36, 51−55, and 63−77.

A representative backbone conformation selected from the calculated structures is shown in Figure 5A as an α-carbon trace with line width varying to reflect circular variance in the ψ torsion angle. This structure consists of two helical regions, one at the N-terminal spanning residues 14−38 and a second at the C-terminal extending from residue 50 to residue 76. A largely disordered region links these two helical domains. The three regions of particularly well-defined helix,

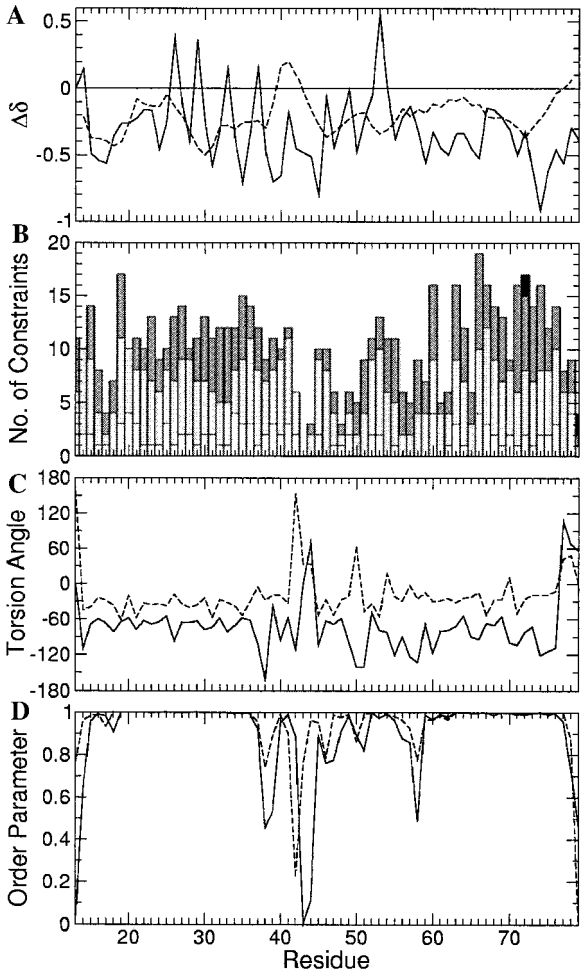

FIGURE 4: (A) Secondary chemical shifts for Hα (- - -) and HN (—) of each residue. Hα shifts are presented as a 3 point running average. (B) The number of distance constraints per residue is presented, with white bars representing intraresidue constraints, pale gray bars representing sequential constraints, dark gray bars representing medium-range ($i - j < 5$) constraints, and black bars representing long-range ($i - j \geq 5$) constraints. The average angle (C) and associated order parameters (D) of the backbone torsion angles ϕ (—) and ψ (- - -) for each residue over the family of 22 calculated structures.

residues 16−36, 50−56, and 63−76, are highlighted in Figure 5A with cylinders.

As has been predicted from primary sequence data, the N-terminal helix is amphipathic, with all of its hydrophobic residues found on one face of the helix (Figure 5B). Charged residues are distributed according to the pattern of class A_2 amphipathic helices (*37*), with negatively charged residues found along the center of the hydrophilic face and positively charged residues at the interface between the hydrophobic and hydrophilic faces. This charge distribution is characteristic of lipid binding regions of apolipoproteins. The hydrophobic face consists of two clusters of hydrophobic residues, the first comprising residues F14, L15, V18, and L22 and the second comprising residues A29, A32, A33, and L36. These two clusters are separated on the hydrophobic face of the helix by aromatic residues Y25 and W26.

These two aromatic residues also mark the location of a pronounced bend in the N-terminal helix. This bend is seen consistently in all 22 of the accepted structures in this study, with its magnitude varying over the range 30−60°. This variation is reflected in the slightly elevated atomic RMSDs

Table 1: Statistics for the Accepted Structures of ApoC-II

	average[a]	best[b]
no. of NOE-derived distance constraints		
total	408	
intraresidue	107	
interresidue	301	
no. of dihedral angle constraints	43	
constraint violations		
no. of distance violations >0.2 Å	1.1 ± 1.0	0
no. of dihedral violations >1°	0	0
largest distance violation (Å)	0.23 ± 0.03	0.178
RMSD from distance constraints (Å)	0.038 ± 0.002	0.034
RMSD from dihedral violations (deg)	0	0
structural energies (kcal/mol)		
total	60 ± 22	7.5
bond	4.4 ± 0.6	3.3
angle	49 ± 4	43
Lennard−Jones	−79 ± 14	−109
distance constraint	44 ± 6	35
backbone atom RMSDs (Å)[c]		
residues 16−36	0.52	
residues 50−56	0.45	
residues 63−77	0.45	

[a] Average values ± standard deviation calculated for the 22 accepted structures. [b] Best values for the 22 accepted structures. [c] Average pairwise RMSDs of atomic coordinates of C′, Cα, and N for indicated residues across 22 accepted structures.

over residues 16−36 (Table 1), as compared to regions 17−25 and 26−36 that have RMSDs of 0.25 and 0.28 Å, respectively. To ensure that this bend is not an artifact of the structure calculation, we modeled this region as a straight helix. This process revealed a number of distance constraints between the α- and side-chain protons of S23 and S24 to the amide of E27 which were inconsistent with such a conformation and are thus direct evidence for the existence of the helical bend. When these constraints are omitted from the structure calculation, structural definition over residues 23−27 is significantly reduced, and no consistent bend in the helix is seen. Although bends have been observed in the structures of several other apolipoprotein lipid binding helices, they are exclusively orientated toward the hydrophobic face. The bend seen here is unique in that it is directed away from the hydrophobic face, making that face convex.

The C-terminal region, which has been implicated in LpL activation, is helical over residues 50−76, with well-defined regions of helix comprising residues 50−54 and 63−76, and a region of less ordered helical structure over residues 55−62. Previous sequence analysis has identified two putative amphipathic helices in this region, the first being a class A_2 helix over residues 44−55 while the second, over residues 60−76, has been designated class G*, reflecting a random distribution of charged residues over the polar face of the helix (*4*). The data presented here define a helical conformation for this second amphipathic region and for the C-terminal half of the first region (Figure 5A). The intervening region also appears to be helical, though with somewhat reduced order. The residues N-terminal of residue 50, despite their amphipathic sequence, are poorly defined in the calculated family of structures and show helical character in only 8 out of 22 structures. Figure 3 reveals very few medium-range NOEs over this region, despite minimal resonance overlap, whereas the Hα secondary chemical shifts are negative and HN secondary shifts show the 3−4 residue periodic variation typical of amphipathic helices. Thus, the current data seem ambiguous with regard to the structure of residues 44−50.

As with the N-terminal amphipathic helix, the hydrophobic face of residues 59−76 can be seen to form two hydrophobic clusters, the first comprising residues A59, M60, Y63, I66, and F67 and a second consisting of V71, L72, V74, and L75 (Figure 6). These clusters are some 120° out of alignment about the helical axis, presenting a substantial deviation from the ideal amphipathic conformation.

At the extreme C-terminal, residues 77−79 have been observed previously to form a turn-like structure (*17*, *18*) in which the glycine at residue 77 adopts an unusual backbone conformation causing E78 and E79 to be bent out and back alongside the helix. This conformation, shown in Figure 5C, caps the helix and prevents these charged residues from impinging on the hydrophobic face of the helix, placing them instead on the hydrophilic face where along with D69 they form an extended acidic surface. Here we see NOEs from the backbone amide of L72 to both the HN and Hα of E79, which, along with a number of sequential and medium-range NOEs, constrain this conformation. Given the lack of any stabilizing tertiary interactions, this is a remarkably well-defined terminal structure, and it has been suggested that this degree of order may be indicative of a functional role for this C-terminal structure, presumably in LpL activation (*18*).

A number of cross-peaks arising as a result of NOEs between apoC-II amides and protons of the SDS fatty acyl chain have also been identified in the $^{1}H,^{15}N$-NOESY−HSQC spectra. Connectivities assigned as such are summarized in Figure 7. These data indicate close interaction between apoC-II and the SDS acyl chains over much of the sequence, particularly the N-terminal helix and residues 48−58. Perhaps surprisingly, these interactions do not display the 3−4 residue periodicity that might be expected for amphipathic helices bound to the surface of the SDS micelle. This may be a result of spin diffusion obscuring the fine detail of the interaction, or it might reflect an alternate mode of interaction between apoC-II and SDS. Also of note is the relative scarcity of SDS contacts to residues N-terminal of the helical bend at residue 25. This suggests that the C-terminal half of the lipid binding helix is more closely associated with SDS than is the N-terminal half. It seems likely that this differential binding arises because the bend prevents interaction of the entire hydrophobic face of the helix with the SDS surface.

DISCUSSION

We have described the structure of human apoC-II in complex with SDS, as determined by NMR spectroscopy. Evidence from CD spectroscopy suggests a helical content of approximately 60% under the conditions studied, and this is consistent with that seen in the structures calculated from NMR-derived constraints, with the ensemble of accepted structures containing some 65% of residues in a helical conformation, including 50% in well-defined regions of α-helix.

The three regions of defined α-helix correspond loosely to the amphipathic regions predicted on the basis of amino acid sequence. The largest of these, comprising residues 16−

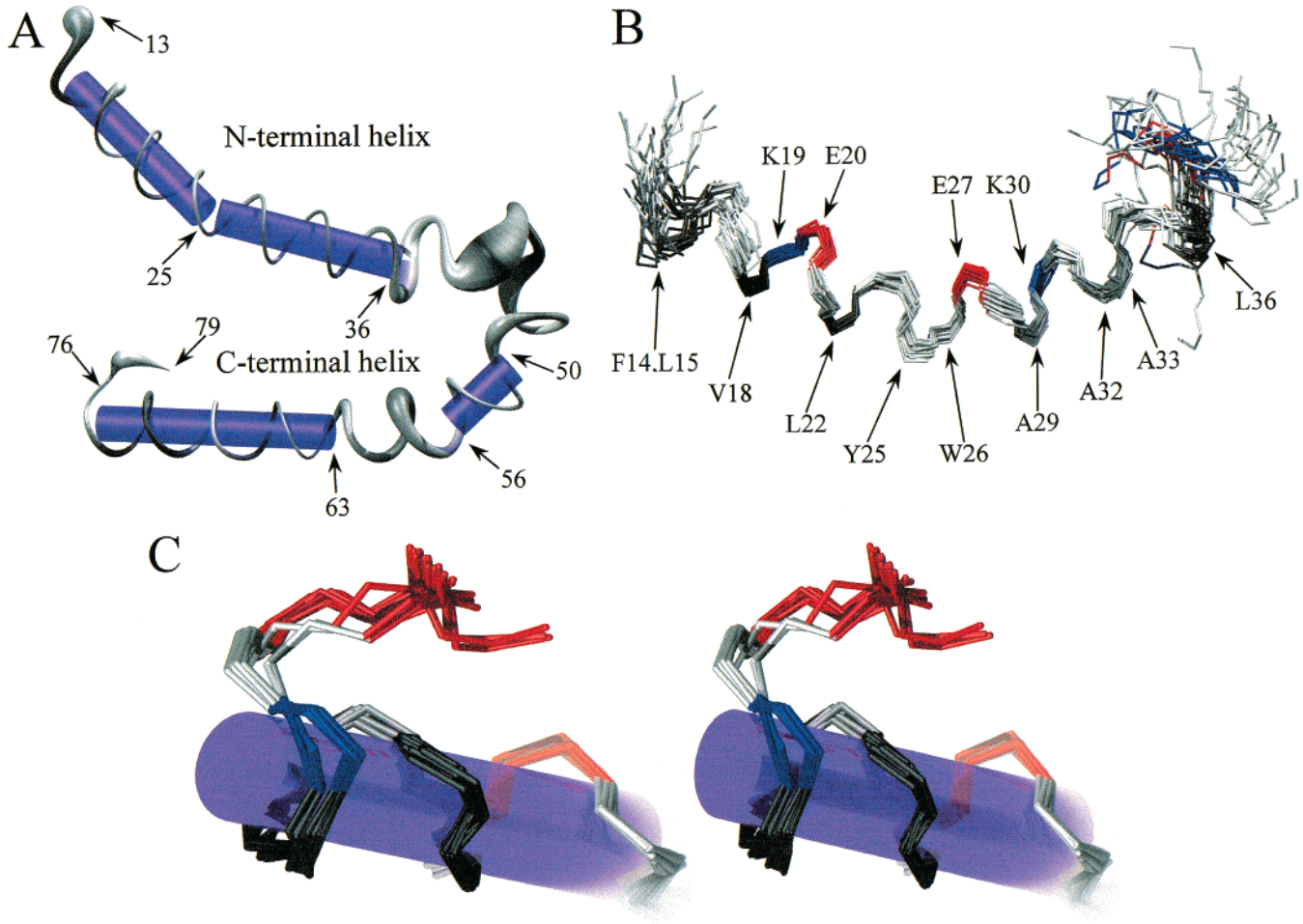

FIGURE 5: (A) Representative calculated structure of apoC-II, presented as an α-carbon trace with the line width drawn to represent angular variance of the ϕ torsion angle over the family of 22 calculated structures. Narrow line width indicates well-defined structure, while broader line width indicates more poorly defined structure. The helical axes of regions of well-defined helicity are indicated with cylinders. The N- and C-terminal helical regions are labeled, as is the position of significant residues (see text for details). (B) The calculated structures of the N-terminal helix of apoC-II, backbone bonds only, superimposed over residues 16−36. Positive and negative residues are shown in blue and red, respectively, while other residues are shaded according to hydrophobicity, with darker shading indicating greater hydrophobicity. (C) Stereoview of the calculated structures of the C-terminus of apoC-II, backbone bonds only, superimposed over residues 65−76. Positive and negative residues are shown in blue and red, respectively, while other residues are shaded according to hydrophobicity, with darker shading indicating greater hydrophobicity.

36, constitutes the proposed lipid binding domain of apoC-II. Like the lipid binding domains of the other exchangeable apolipoproteins, this is a class A_2 amphipathic α-helix with two lysine residues, K19 and K30, lying at the interface between the hydrophilic and hydrophobic faces, and the negatively charged residues E20 and E27 in the middle of the hydrophilic face (Figure 5B). Despite extensive study, the role of this charge distribution in lipid binding remains controversial (*4*).

The hydrophobic face of the N-terminal helix consists of two clusters of hydrophobic residues similar to those described in the lipid binding regions of apoC-I (*38*). In sharp contrast to apoC-I and other apolipoprotein lipid binding regions, however, the bend that separates the two hydrophobic clusters makes the hydrophobic face convex. This appears counterintuitive on the basis of the assumption that apoC-II binds to the curved surface of the SDS micelle in a similar way as it is presumed to bind to the lipoprotein surface in vivo. This model of the SDS−apoC-II interaction would suggest a concave hydrophobic face that follows the curvature of the micelle surface, and such curvature is reported for many of the apolipoprotein lipid binding helices for which structures are available. It should be noted, however, that apoC-II is found largely on the larger lipoprotein species, the chylomicrons and very low-density lipoproteins (*39*). It may be that the convex hydrophobic face of the apoC-II lipid binding region is responsible for the preference of apoC-II for the less curved lipid surfaces of the larger lipoproteins. Such a proposition is supported by the observation that the C-terminal half of the lipid binding helix appears to preferentially interact with the SDS micelle (Figure 7), which has radius some 10 times smaller than typical of very low-density lipoprotein particles. Presumably a less curved lipid surface would interact with a larger proportion of the hydrophobic face of the lipid binding region. It is also possible that this unusual curvature results from specific SDS-mediated effects rather than reflecting the native lipoprotein-bound conformation. For this reason, it is important that the structural studies presented here be extended into other lipid systems. The importance of W26, which falls on the outside face of this bend, in the function of apoC-II is underlined by the apoC-II-Wakayama mutation.

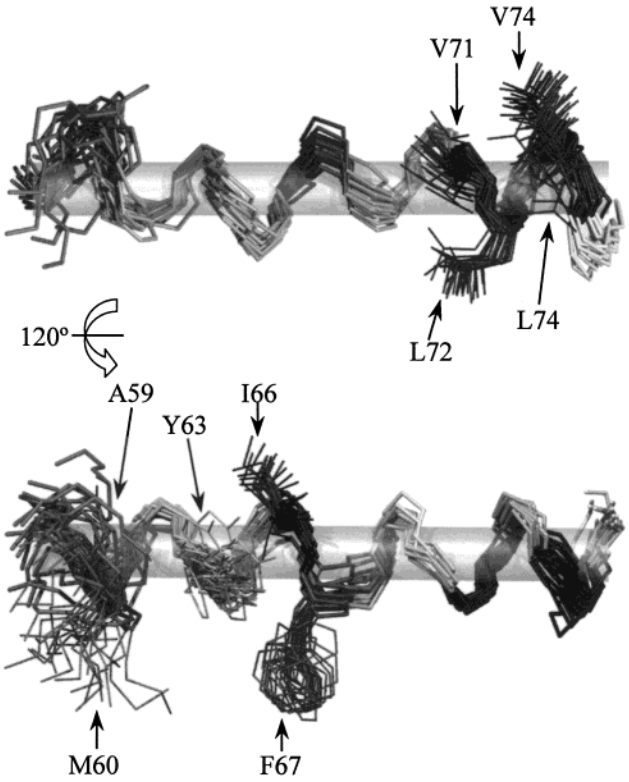

FIGURE 6: Calculated structures of residues 58−76 of apoC-II, shown in two orientations rotated 120° about the helical axis with respect to each other. Side chains of the two hydrophobic clusters are shown, with residues 71, 72, 74, and 75 shown on the front face of the helix in the first representation. The second representation shows side chains of residues 59, 60, 63, 66, and 67 oriented toward the front. Bonds are shaded according to hydrophobicity, with darker shading indicating greater hydrophobicity.

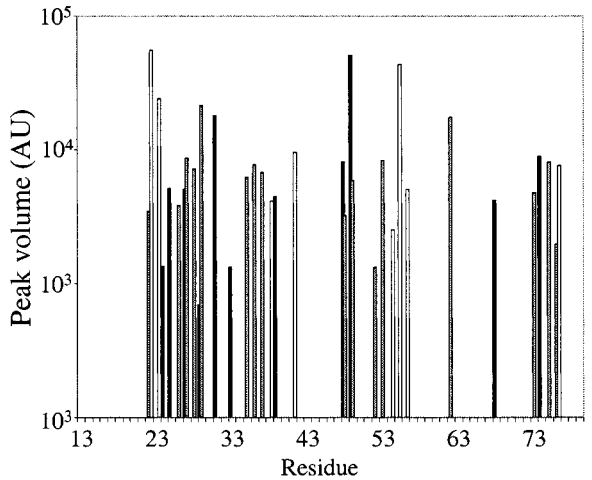

FIGURE 7: Sequence distribution of NOE cross-peaks between apoC-II backbone amides and protons of the SDS fatty acid chains. NOEs to protons on C2 of SDS are represented in white, those to protons on C3−C11 are in gray, and those to the methyl protons on C12 are in black.

In this form of apoC-II, an arginine is substituted at this position, resulting in an apoC-II deficiency (*40*).

The C-terminal half of apoC-II contains two regions of defined α-helix, residues 50−54 and 63−76, with an intervening region of less-ordered helical structure (Figure 5A). Both of the defined helical regions are amphipathic, and have been previously identified as putative helical regions on the basis of amino acid sequence. This structure can be compared to that determined previously for peptides corresponding to residues 50−79 in 35% HFP (*17*) and residues 44−79 in SDS (*18*). Both previous structures are in agreement with the one presented here with regard the conformation of residues C-terminal of F67, namely, a defined helix C-terminally capped by a turn-like structure. In the present structure, this helix continues toward the N-terminal at least as far as residue 63, whereas both peptide structures indicate regions of disorder between residues 59 and 68. The structure of the longer peptide also includes a moderately well-defined helix over residues 50−58, in agreement with the conformation presented here.

Studies of peptides derived from the C-terminal half of apoC-II have shown that neither of the putative helices in isolation interact with phospholipid surfaces (*5*, *9*), but a peptide encompassing both helices does form peptide−phospholipid complexes (*7*), suggesting the importance of cooperativity in the lipid binding of the C-terminus. The structure described here suggests possible reasons for this lack of lipid binding activity in the individual helices. Despite a strongly amphipathic amino acid sequence over residues 44−55, defined helical conformation is observed only for residues 50−54, suggesting that this region lacks a hydrophobic face large or stable enough to possess significant lipid affinity. The C-terminal helix, on the other hand, is well-defined over 14 residues, forming hydrophobic clusters containing at least 7 bulky hydrophobic or aromatic residues. Its lack of lipid affinity in isolation appears to be due to the misalignment of the two hydrophobic clusters about the helical axis. This misalignment is evident from the amino acid sequence, with the hydrophobic moment of residues 59−67 making an angle of 111° with that of residues 71−75 when calculated assuming an ideal α-helical conformation over residues 59−75.

The distortion to ideal amphipathic conformation may well play a role in LpL activation given the importance attributed to this region in that function of apoC-II. Such a role might involve the disruption of the lipoprotein surface caused by the misaligned hydrophobic clusters, allowing LpL access to the triacylglycerol core of the lipoprotein. It is also possible that the misalignment allows one hydrophobic cluster to bind the lipoprotein surface while the other interacts with a hydrophobic region on the LpL surface.

A number of deletion mutagenesis and competition studies have implicated residues KGEE at the extreme C-terminal of apoC-II in LpL interaction and activation (*41*). The apparently stable conformation adopted by these residues appears to support such a contention. This conformation alters the arrangement of charged residues about the C-terminal helix such that it somewhat resembles a class A_2 amphipathic helix, with the acidic face formed by D69, E78, and E79 above the hydrophilic face and the positive charge of K76 at the amphipathic interface (Figure 6). Recent studies of chimeric molecules derived from LpL and the closely related hepatic lipase identified the final 60 C-terminal residues as having a role in the different heparin affinities and apoC-II interactions of the two lipases (*42*). On this basis, it can be speculated that the acidic face at the C-terminal of apoC-II might interact with the putative basic surfaces of the C-terminal of LpL as part of the activation mechanism.

ADDED IN PROOF

The coordinates of the 22 accepted structures have been deposited in the RCSB Protein Data Bank (PDB entry 1I5J).

ACKNOWLEDGMENT

We are grateful to Dr. James Swarbrick for assistance with spectral analysis.

SUPPORTING INFORMATION AVAILABLE

A table of chemical shifts for all assigned atoms is available as Supporting Information (4 pages). This material is available free of charge via the Internet at http://pubs.acs.org.

REFERENCES

1. Havel, R. J., Fielding, C. J., Olivecrona, T., Shore, V. G., Fielding, P. E., and Egelrud, T. (1973) *Biochemistry 12*, 1828−1833.
2. Jackson, R. L., and Holdsworth, G. (1986) *Methods Enzymol. 128*, 288−297.
3. Tajima, S., Yokoyama, S., Kawai, Y., and Yamamoto, A. (1982) *Biochem. J. 91*, 1273−1279.
4. Segrest, J. P., Jones, M. K., De Loof, H., Brouillette, C. G., Venkatachalapathi, Y. V., and Anantharamaiah, G. M. (1992) *J. Lipid Res. 33*, 141−166.
5. Catapano, A. L., Kinnunen, P. K., Breckenridge, W. C., Gotto, A. M., Jr., Jackson, R. L., Little, J. A., Smith, L. C., and Sparrow, J. T. (1979) *Biochem. Biophys. Res. Commun. 89*, 951−957.
6. MacPhee, C. E., Howlett, G. J., Sawyer, W. H., and Clayton, A. H. A. (1999) *Biochemistry 38*, 10878−10884.
7. Smith, L. C., Voyta, J. C., Catapano, A. L., Kinnunen, P. K., Gotto, A. M., Jr., and Sparrow, J. T. (1980) *Ann. N.Y. Acad. Sci. 348*, 213−223.
8. Clarke, A. R., and Holbrook, J. J. (1985) *Biochim. Biophys. Acta 827*, 358−368.
9. MacPhee, C. E., Hatters, D. M., Sawyer, W. H., and Howlett, G. J. (2000) *Biochemistry 39*, 3433−3440.
10. Hatters, D. M., MacPhee, C. E., Lawrence, L. J., Sawyer, W. H., and Howlett, G. J. (2000) *Biochemistry 39*, 8276−8283.
11. Soutar, A. K., Hawkins, P. N., Vigushin, D. M., Tennent, G. A., Booth, S. E., Hutton, T., Nguyen, O., Totty, N. F., Feest, T. G., Hsuan, J. J., and Pepys, M. B. (1992) *Proc. Natl. Acad. Sci. U.S.A. 89*, 7389−7393.
12. Higuchi, K., Kogishi, K., Wang, J., Xia, C., Chiba, T., Matsushita, T., and Hosokawa, M. (1997) *Biochem. J. 325*, 653−659.
13. Levin, M., Pras, M., and Franklin, E. C. (1973) *J. Exp. Med. 138*, 373−380.
14. Mucchiano, G., Cornwell, G. G., and Westermark, P. (1992) *Am. J. Pathol. 108*, 135−139.
15. Westermark, P., Mucchiano, G., Marthin, T., Johnson, K. H., and Sletten, K. (1995) *Am. J. Pathol. 147*, 1186−1192.
16. Lycksell, P.-O., Ohman, A., Bengtsson-Olivecrona, G., Johansson, L. B., Wijmenga, S. S., Wernic, D., and Graslund, A. (1992) *Eur. J. Biochem. 205*, 223−231.
17. Ohman, A., Lycksell, P.-O., and Graslund A. (1993) *Eur. Biophys. J. 22*, 351−357.
18. Storjohann, R., Rozek, A., Sparrow, J. T., and Cushley, R. J. (2000) *Biochim. Biophys. Acta 1486*, 253−264.
19. Opella, S. J. (1997) *Nat. Struct. Biol. 4 Suppl.*, 845−848.
20. Wang, C. S., Downs, D., Dashti, A., and Jackson, K. W. (1996) *Biochim. Biophys. Acta 1302*, 224−230.
21. Cai, M., Huang, Y., Sakaguchi, K., Clore, G. M., Gronenborn, A. M., and Craigie, R. (1998) *J. Biol. NMR 11*, 97−102.
22. Morriset, J. D., David, J. S. K., Pownall, H. J., and Gotto, A. M. (1973) *Biochemistry 12*, 1290−1299.
23. Bodenhausen, G., and Ruben, D. J. (1980) *Chem. Phys. Lett. 69*, 185−189.
24. Fesik, S. W., and Zuiderweg, E. R. P. (1988) *J. Magn. Reson. 78*, 588−593.
25. Marion, D., Kay, L. E., Sparks, S. W., Torchia, D. A., and Bax, A. (1989) *J. Am. Chem. Soc. 111*, 1515−1517.
26. Vuister, G. W., and Bax, A. (1993) *J. Am. Chem. Soc. 115*, 7772−7777.
27. Zhang, O., Kay, L. E., Olivier, J. P., and Forman-Kay, J. D. (1994) *J. Biomol. NMR. 4*, 845−858.
28. Archer, S. J., Ikura, M., Torchina, D. A., and Bax, A. (1991) *J. Magn. Reson. 95*, 636−641.
29. Frenkiel, T., Bauer, C., Carr, M. D., Birdsall, B., and Feeney, J. (1990) *J. Magn. Reson. 90*, 420−425.
30. Piotto, M., Saudek, V., and Sklenar, V. (1992) *J. Biol. NMR 2*, 661−665.
31. Delaglio, F., Grzesiek, S., Vuister, G. W., Zhu, G., Pfeifer, J., and Bax, A. (1995) *J. Biomol. NMR 6*, 277−293.
32. Bartels, C., Xia, T. H., Billeter, M., Güntert, P., and Wüthrich, K. (1995) *J. Biomol. NMR 6*, 1−10.
33. Wüthrich, K. (1986) *NMR of Proteins and Nucleic Acids*, Wiley, New York.
34. Güntert, P., Mumenthaler, C., and Wüthrich, K. (1997) *J. Mol. Biol. 273*, 283−298.
35. Brunger, A. T., Adams, P. D., Clore, G. M., DeLano, W. L., Gros, P., Grosse-Kunstleve, R. W., Jiang, J. S., Kuszewski, J., Nilges, M., Pannu, N. S., Read, R. J., Rice, L. M., Simonson, T., and Warren, G. L. (1998) *Acta Crystallogr., Sect. D: Biol. Crystallogr. 54*, 905−921.
36. Fojo, S. S., Taam, L., Fairwell, T., Ronan, R., Bishop, C., Meng, M. S., Hoeg, J. M., Sprecher, D. L., and Brewer, H. B., Jr. (1986) *J. Biol. Chem. 261*, 9591−9594.
37. Segrest, J. P., De Loof, H., Dohlman, J. G., Brouillette, C. G., and Anantharamaiah, G. M. (1990) *Proteins: Struct., Funct., Genet. 8*, 103−117.
38. Rozek, A., Buchko, G. W., Kanda, P., and Cushley, R. J. (1997) *Protein Sci. 6*, 1858−1868.
39. Wang, C.-S. (1991) *Prog. Lipid Res. 30*, 253−258.
40. Kuniyoshi, A., Okamoto, Y., Tamagawa, T., Matsuyama, Y., and Fuku, H. (1999) *Intern. Med. 38*, 140−144.
41. Kinnunen, P. K., Jackson, R. L., Smith, L. C., Gotto, A. M., Jr., and Sparrow, J. T. (1977) *Proc. Natl. Acad. Sci. U.S.A. 74*, 4848−4851.
42. Hill, J. S., Yang, D., Nikazy, J., Curtiss, L. K., Sparrow, J. T., and Wong, H. (1998) *J. Biol. Chem. 273*, 30979−30984.

BI002821M